Available online at www.sciencedirect.com
ScienceDirect
Combustion and Flame 151 (2007) 196–208
Combustion and Flame
www.elsevier.com/locate/combustflame

A study of the effects of diluents on near-limit H_2–air flames in microgravity at normal and reduced pressures

L. Qiao [a,*], Y. Gu [a], W.J.A. Dahm [a], E.S. Oran [b], G.M. Faeth [a]

[a] *Department of Aerospace Engineering, The University of Michigan, Ann Arbor, MI 48109-2140, USA*
[b] *Laboratory for Computational Physics and Fluid Dynamics, Naval Research Laboratory, Washington, DC 20375, USA*

Received 5 October 2006; received in revised form 31 May 2007; accepted 12 June 2007

Available online 3 August 2007

Abstract

A combination of microgravity experiments and computational simulations were used to study effects of diluents on the near-limit properties of laminar, premixed hydrogen/air flames. The experiments were conducted in a short-drop free-fall laboratory facility that provided at least 450 ms of $10^{-2}g$ conditions. Outwardly propagating spherical flames were used to measure near-limit laminar burning velocities at various fuel-equivalence ratios and pressures with reactants containing varying concentrations of He, Ar, N_2, and CO_2 as fire suppressants. Burning velocities were also computed using the steady, one-dimensional laminar premixed flame code PREMIX with detailed chemical kinetics, transport properties, and radiative heat loss based on an optically thin assumption. Measured and computed results both showed the suppressant effectiveness to increase in the order He, Ar, N_2, and CO_2. This is attributed to both the increasing specific heats and the decreasing transport rates of the gases. The suppressants can also decrease the Markstein number, especially for CO_2, causing the flames to become more susceptible to preferential-diffusion instability. The resulting increase in flame surface wrinkling increases the burning velocity, thus counteracting the desired effect of the flame suppressant. The agreement between measured and computed laminar burning velocities was better than it was near the limit. Sensitivity analyses suggest that inaccuracies in three-body termination rates for $H + O_2 + M = HO_2 + M$ reactions and in mass diffusion coefficients for H_2 diffusion are the most likely explanation for the near-limit differences.

Keywords: Extinction; Diluents; Hydrogen flames; Microgravity

1. Introduction

Chemically inert diluents are an important class of fire extinguishing agents because of their relatively benign effects on people and equipment. Such diluents may be essential, for example, for extinguishing fires in confined environments such as spacecraft. Long-duration missions in particular, including proposed trips to the moon or Mars, substantially increase the risk of accidental fires, and thus development of effective fire-safety systems and procedures for their use in spacecraft environments can be critical in such applications. Chemically active agents, such as halons, have been widely used for both terrestrial and spacecraft applications, and numerous

* Corresponding author. Currently at School of Aeronautics & Astronautics, Purdue University, West Lafayette, IN 47907, USA.
E-mail address: lqiao@umich.edu (L. Qiao).

0010-2180/$ – see front matter
doi:10.1016/j.combustflame.2007.06.013

Nomenclature

D	mass diffusivity
K	flame stretch
K_p	Planck mean absorption coefficient
L	Markstein length
Ma	Markstein number, L/δ_D
P	pressure
r_f	flame radius
S_L	local laminar burning velocity
$S_{L\infty}$	planar unstretched laminar burning velocity
T	temperature
T_0	ambient temperature
t	time
X	mole fraction
δ_D	characteristic flame thickness, $D_u/S_{L\infty}$
ρ	density
ϕ	fuel-equivalence ratio

Subscripts

b	burned gas
i	species i
u	unburned gas
∞	unstretched flame condition

studies have been conducted to understand how they inhibit reactions. Unfortunately, halons can deplete stratospheric ozone. As a consequence their use is being increasingly restricted. Moreover, in confined environments such as spacecraft, halons generate reaction products that damage life-support systems and are difficult to remove from the interior atmosphere. As a result, chemically inert diluents are potentially more suitable for use in such applications.

In a previous study [1], we reported results on the effectiveness of various diluents at relatively low concentrations for outwardly propagating, spherical, premixed flames under normal-gravity conditions. The diluents considered were helium, argon, nitrogen, and carbon dioxide. They were chosen to allow separate identification of the relative effects of dilution, heat capacity, and transport properties. The normal-gravity conditions, however, limited that study to examining flame propagation velocities at relatively low diluent concentrations, for which the resulting flames were sufficiently fast so that buoyancy effects can be neglected. As diluent concentrations increase and the extinction limit is approached, however, the normal-gravity flames in Ref. [1] cannot be used to investigate the near-limit properties and flammability limits that are essential to characterizing flame-suppression effectiveness under microgravity conditions.

Motivated by this, we designed and built a short-drop free-fall facility in the laboratory to eliminate the intrusion of buoyancy on near-extinction flames, which was reported in Ref [2]. Flame behavior was compared in normal gravity and microgravity. The results show that near-extinction flames in normal gravity propagate upward and form a classic mushroom shape due to buoyancy. The resulting non-spherical shape limits accurate determination of the laminar burning velocity. Using a microgravity facility, however, these slow near-limit flames were shown to maintain a highly spherical shape that allowed their laminar burning velocity to be accurately inferred from measurements of the resulting flame radius versus time. The measured and computed near-limit burning velocities $S_{L\infty}$ under microgravity conditions were reported for stoichiometric H_2/air/diluent flames at normal temperature and pressure. It was found that the agreement between measured and computed laminar burning velocities was better than it was near the limit.

Here we extend these earlier studies by presenting more measurements of near-limit burning velocities under microgravity conditions for H_2/air/diluent flames at various fuel-equivalence ratios and pressures. We then compare the measured $S_{L\infty}$ values to computations with detailed chemistry and transport properties and an optically thin radiation model and show that they agree reasonably well far away from the flammability limit, but that they deviate consistently in the near-limit region. We also discuss the effects of the diluents on the preferential-diffusion instability for H_2/air flames. It is shown that the addition of the diluents (except helium) generally decreases the Markstein numbers, which makes the flames more susceptible to preferential-diffusion instability that can partially offset the effectiveness of the diluents in decreasing the flame propagation rate. Finally, we analyze possible causes for the observed discrepancies in the near-limit laminar burning velocities from the experiments and computations from the perspective of chemical kinetics and molecular diffusion, respectively.

2. Experimental methods

The low-gravity experiment duration required for the premixed flames investigated here is not long, and can be achieved in a short-drop (1-m) free-fall facility. In particular, a 1-m free-fall distance provides roughly

450 ms of low-gravity conditions. Since the slowest flames measured herein have a laminar burning velocity of 5 cm/s and the distance of flame propagation for the present conditions is roughly 30 mm, the flame propagation time is roughly 120 ms, leaving roughly 330 ms for contingencies such as ignition delay times. The 1-m free-fall system thus provides a simple yet effective arrangement with fast experimental turn-around times.

The experimental methods are similar to earlier work [2] and will be described only briefly here (see [2] for more details). The free-fall facility consists of a support tower, a free-falling spherical combustion chamber, a spark generator, a deceleration box, and shadowgraph optics that record the flame propagation as the chamber falls. The free-fall chamber was held at the top of the tower by an electromagnet before being dropped. As the chamber was released, a Hall-effect sensor detected the motion and sent a trigger pulse to the delay generator. A short delay was then provided to allow oscillations from the chamber release to decay to sufficiently low levels. After the delay, the generator sent out two signals, one of which triggered a high-voltage spark generator connected to electrodes that ignited the mixture, and the other of which triggered a high-speed digital video camera that recorded shadowgraph images of the flame propagation within the free-falling chamber. The two electrodes that generated a spark at the center of the chamber consisted of 250-μm-diameter tungsten wires having free lengths of 40 mm. The spark gap was adjusted from 0.5 to 3.0 mm, with larger gaps used to ignite flames having high diluent concentrations that require larger ignition energies. The spark energy was supplied by a high-voltage capacitive discharge circuit with an adjustable voltage of 0–30 kV and a discharge time of roughly 5 μs. The spark gap and spark energy were adjusted to be as close as possible to the minimum ignition energies.

The present measurements were restricted to flames having diameters 10 mm $< d <$ 60 mm. The lower limit provides sufficient time for disturbances introduced by ignition to decay, while the upper limit limits the pressure rise in the chamber during the measuring period to less than 0.7% of the initial pressure. No results were considered where the flame surface was found to be wrinkled due to flame instabilities. Similar to previous measurements of laminar premixed flame properties [1,2], measurements were also limited to $\delta_D/r_f < 0.05$, where δ_D is the characteristic flame thickness and r_f is the flame radius, so that effects of curvature and transient phenomena associated with large flame thickness during the early stages of flame formation were small. Under these assumptions, quasi-steady expressions for the local laminar burning velocity and flame stretch are given by [3]

$$S_L = \frac{\rho_b}{\rho_u}\frac{dr_f}{dt}, \qquad K = \frac{2}{r_f}\frac{dr_f}{dt}, \tag{1}$$

where S_L is the observed stretched flame propagation speed into the unburned gas and K is the flame stretch. The density ratio needed to find S_L was computed assuming adiabatic constant-pressure combustion with the same concentrations of elements in the unburned gases. These calculations were carried out using the adiabatic equilibrium algorithms of McBride et al. [4]. This approach ignores preferential-diffusion effects that modify the local mixture fractions and thermal energy transport and cause local changes of the density ratios of stretched flames. This approach is convenient, however, because a single density ratio relates all flame speeds under a given reactant mixture condition. The flame propagation velocity, dr_f/dt, was obtained from the flame radius $r_f(t)$ as measured from the shadowgraph images along the direction perpendicular to the spark electrodes, where disturbances of the flame surface by the electrodes were minimal.

From Markstein [5] and Clavin [6], the laminar burning velocity S_L is related to the flame stretch K for small to moderate values of curvature and stretch,

$$S_L = S_{L\infty} - LK. \tag{2}$$

The Markstein length L is a measure of the flame response to the stretch rate K and can be either positive (preferential-diffusion stable) or negative (preferential-diffusion unstable), depending on the reactants. The unstretched laminar burning velocities $S_{L\infty}$ were obtained by extrapolating the measured stretched laminar burning velocities $S_L(K)$ as a function of the local stretch rate K to zero stretch. The Markstein length is proportional to a characteristic flame thickness, δ_D, so that a dimensionless Markstein number can be defined as

$$\mathrm{Ma} = L/\delta_D = L/(D_u/S_{L\infty}) = LS_{L\infty}/D_u. \tag{3}$$

Here, δ_D is defined as the ratio of mass diffusivity D_u to $S_{L\infty}$, where D_u is the mass diffusivity of the fast-diffusing species H_2 to the reactant mixture. Final results were averaged over measurements from three to five tests under each condition, with 95% confidence intervals characterizing uncertainties in the reported values. Experimental uncertainties (95% confidence) in the present flame radius r_f and time t were estimated to be less than 3 and 1%, respectively. The corresponding uncertainties in dr_f/dt and K were less than 4.5 and 5.4%, respectively. The ratios of ρ_u/ρ_b were assumed to be known, so that they did not contribute to uncertainty estimates. This implies that the uncertainty in S_L was the same as that in dr_f/dt, and

thus was less than 4.5%. Finally, the uncertainties in $S_{L\infty}$ and Ma were determined from the linear extrapolation of S_L and K. Generally, the uncertainty for $S_{L\infty}$ was found to be less than 12% and that for Ma was less than 25%, with larger uncertainties for the conditions where the value of Ma was close to zero.

3. Computational methods

Numerical calculations of the corresponding planar unstretched premixed flames were carried out using the steady, one-dimensional laminar premixed flame code PREMIX [7]. This code allows for multicomponent diffusion, thermal diffusion, variable thermochemical properties, and variable transport properties. This is presumed to be a sufficiently accurate treatment of transport for the present purposes. The numerical algorithm employs self-adaptive griding to deal with regions where property gradients are large. The computational grid in space was varied to ensure numerical accuracy. The present calculations used the updated comprehensive kinetic model for hydrogen combustion due to Li et al. [8]. CHEMKIN was used as a preprocessor to determine thermochemical and transport properties from the database of Kee et al. [9], except for HO_2, for which the recommendations of Kim et al. [10] were used.

Previous studies [11,12] have shown that the effect of radiative heat loss is small compared to the total heat release rate and can be neglected for fast-propagating hydrogen flames. As the flame propagation becomes slower, however, radiative heat losses become increasingly important and lead to lower burning velocities and flame temperatures. Here we assumed optically thin flames so that the volumetric rate of radiation heat loss in the energy equation could be written as

$$q_r = -4\sigma K_p\left(T^4 - T_0^4\right), \tag{4}$$

where σ is the Stefan–Boltzmann constant, K_p is the Planck mean absorption coefficient of the mixture, and T and T_0 are local and ambient temperature, respectively. The value of K_p was calculated locally from T and the mole fraction of each species according to

$$K_p = \sum_i P_i K_{p,i}, \tag{5}$$

where P_i and $K_{p,i}$ are the partial pressure and Planck mean absorption coefficient of species i. In the present study, the major radiating species were assumed to be H_2O and CO_2. The values of $K_{p,i}$ were taken from the work by Ju et al. [13]. They were calculated based on the statistical narrowband model (SNB) with exponential-tailed inverse line strength distribution. The resulting computed unstretched burning velocities $S_{L\infty}$ were compared for each suppressant type and concentration with the corresponding measured values obtained as described above.

4. Laminar burning velocities

The laminar burning velocities presented here are unstretched values, $S_{L\infty}$, determined by applying Eq. (2) to the measured values of S_L and K. These are here referred to as the "measurement-derived values of $S_{L\infty}$," because they are based on experimentally measured values of S_L. Flame radius as a function of time is shown in Fig. 1, for stoichiometric hydrogen/air flames at various diluent (nitrogen) mole fractions and NTP. The flame speed (dr_f/dt) was obtained from the flame radius–time data using the locally weighted fitting program, called LOWESS [14]. The density ratio ρ_u/ρ_b was calculated using the adiabatic equilibrium algorithms of McBride et al. [4]. The resulting laminar burning velocities are shown as a function of flame stretch rate in Fig. 2.

Our experimental observations show that for all flames, when $S_{L\infty}$ exceeds 20 cm/s, gravity effects can be neglected and the observed flame propagation is essentially the same at $1g$ and μg. As $S_{L\infty}$ gets lower, however, gravity effects become more important and the flame kernel moves upward. The dimensionless Richardson number Ri, a measure of the relative importance of gravity [15], is defined as $\mathrm{Ri} = (\Delta\rho/\rho)gd/S_{L\infty}^2$, where the ratio of density difference $\Delta\rho/\rho$ is close to unity for most flames, g is the acceleration of gravity, and d is the maximum flame diameter we measured. Thus we get a critical value of $\mathrm{Ri} \approx 15$ based on the critical burning velocity 20 cm/s. This means that when $\mathrm{Ri} < 15$, gravity effects can be neglected for the premixed flames investigated here.

The resulting measured and computed laminar burning velocities as a function of the mole concentration of diluents for H_2/air mixtures are shown in Figs. 3–6 for various diluents, fuel-equivalence ratios, and pressures. The oxygen index, which is the concentration of oxygen (in %) by volume in the nonfuel gas, is a single-valued function of diluent concentration for the conditions of Figs. 3–6 and is shown as an independent variable in these figures. The measured laminar burning velocities for diluent mole fractions below 40% are from previous $1g$ experiments [1]. Since the burning velocities in those cases generally exceed 20 cm/s, gravity effects can be neglected and direct comparisons with the present microgravity results can be made. For diluent volume fractions above

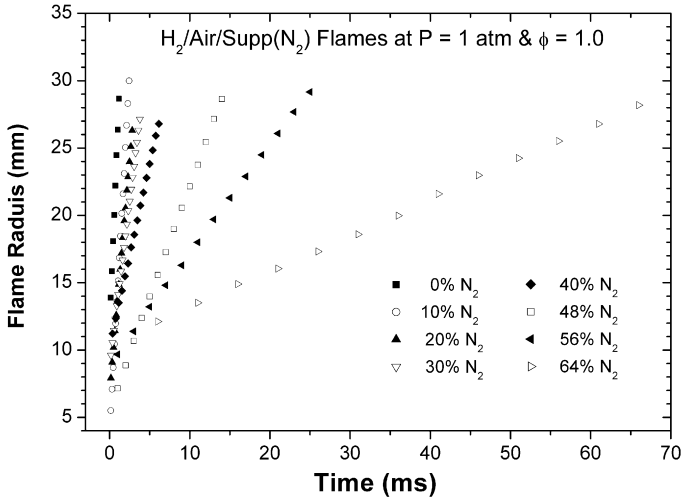

Fig. 1. Measured variation of flame radius with elapsed time for stoichiometric H_2/air/supp (N_2) flames at NTP and various suppressant mole fractions.

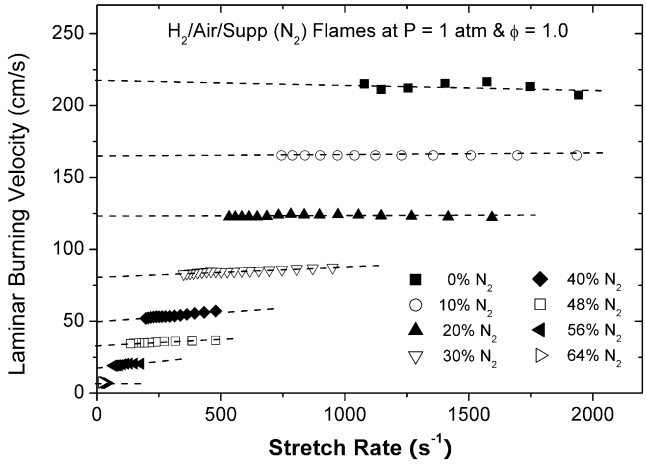

Fig. 2. Measured variations of laminar burning velocities with stretch rate for stoichiometric H_2/air/supp (N_2) flames at NTP and various suppressant mole fractions.

40%, in most cases the normal-gravity flame was not sufficiently spherical to obtain meaningful values of the flame radius, and thus laminar burning velocities are reported only from the microgravity measurements. The uncertainties in the measured laminar burning velocities are shown by 95% confidence intervals.

Fig. 3, taken from Ref. [2], shows the measured and predicted laminar burning velocities as a function of the molar concentration of diluents for stoichiometric H_2/air flames at normal temperature and pressure (NTP). The results in Fig. 3 show that all diluents considered here cause $S_{L\infty}$ to decrease as the diluent concentration is increased. The relative effectiveness of the diluents is defined as the fractional reduction of $S_{L\infty}$ at any fixed diluent concentration relative to its undiluted value. The effectiveness increases in the order He < Ar < N_2 < CO_2, with CO_2 being most effective. This can be explained by their increasing specific heats to absorb heat; that is, the inert suppressants Ar (or He), N_2, and CO_2 progressively reduce flame temperatures and thus reduce flame speeds. This conclusion is similar to that found in the previous work by Saito et al. [16] and Saso et al. [17], in which the fire extinguishing efficiency of Ar, N_2, and CO_2 was investigated for premixed hydrocarbon fuels. $S_{L\infty}$ for He, however, is much greater than that for Ar, although they have approximately equal specific heats, which means their flame temperatures are about equal. This is due to the much higher thermal diffusivity of He, resulting in a higher burning velocity for He than for Ar. We conclude that the

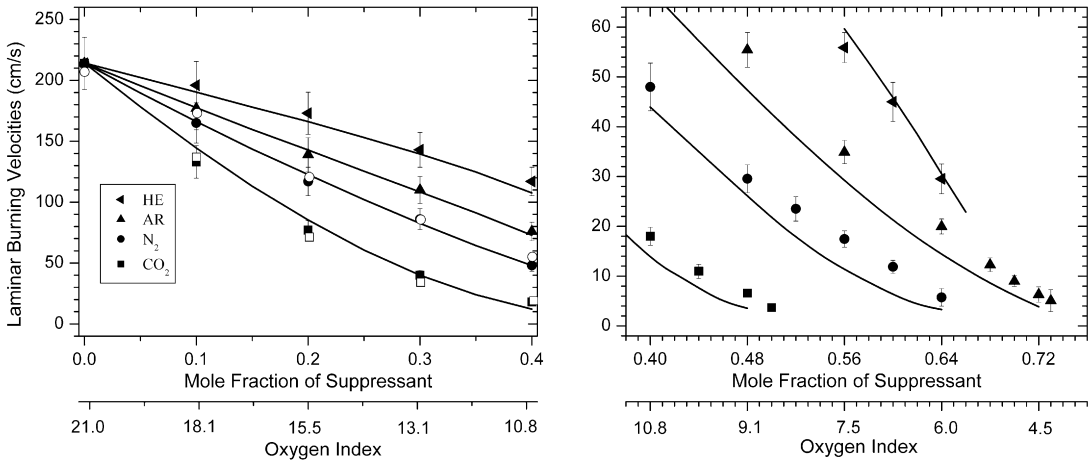

Fig. 3. Measured (symbols) and computed (lines) planar laminar burning velocities as a function of the mole fractions of He, Ar, N_2, and CO_2 suppressants for premixed stoichiometric H_2/air/suppressant flames at a pressure of 1.0 atm, obtained from measurements in 1g (left) and μg (right). Taken from Ref. [2].

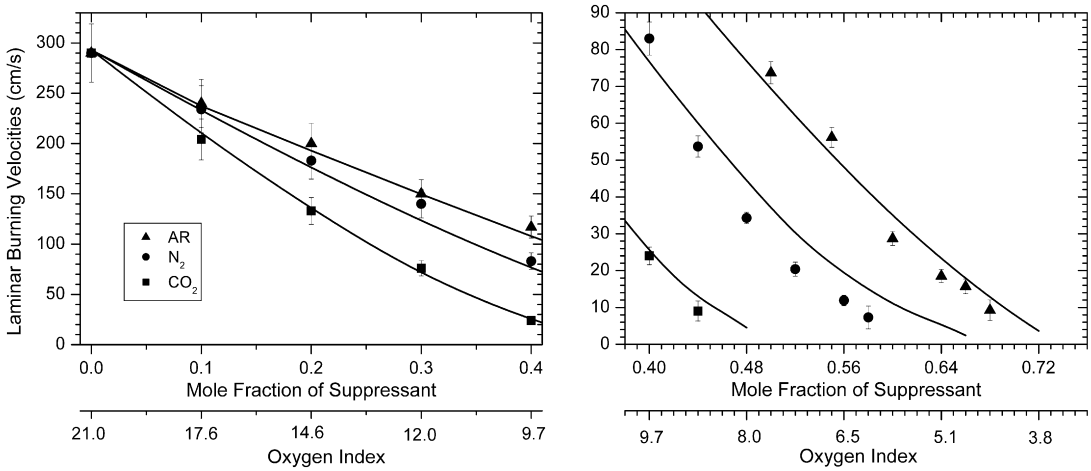

Fig. 4. Measured (symbols) and computed (lines) planar laminar burning velocities as a function of the mole fractions of Ar, N_2, and CO_2 suppressants for premixed H_2/air/suppressant flames at a fuel-equivalence ratio of 1.8 and a pressure of 1.0 atm, obtained from measurements in 1g (left) and μg (right).

relative ranking of suppressant effectiveness depends on both the heat capacity and the transport rates of the diluents. Takahashi et al. [18] investigated the extinction process of diffusion flames by the same diluents, which were introduced into the oxidizer stream. They found the relative ranking of suppressant effectiveness is $CO_2 > N_2 \approx He > Ar$, according to the minimum extinguishing concentration of each diluent. In contrast to our conclusion, their results show that helium is more effective than argon. This is because addition of helium leads to greater heat losses from the downstream diffusion region of the flame than addition of argon, due to the higher thermal conductivity of helium. Overall, the high transport rates of helium have different effects on premixed and diffusion flames.

Fig. 4 shows measured and predicted values of $S_{L\infty}$ as a function of the mole fraction of diluents for H_2/air flames at a fuel-equivalence ratio of 1.8 and NTP. The ratio $\phi = 1.8$ was chosen because it represents conditions where the value of $S_{L\infty}$ for H_2/air mixtures reaches a maximum [11,12,19]. This has been explained based on the high concentration of H in the reaction zone [11]. Figs. 3 and 4 show that the results for $\phi = 1.0$ and 1.8 have similar trends. All diluents cause $S_{L\infty}$ to decrease as the diluent concentration is increased. The relative effectiveness of suppressants increases in the same order from Ar to N_2 to CO_2, due to their increasing heat capacity. We

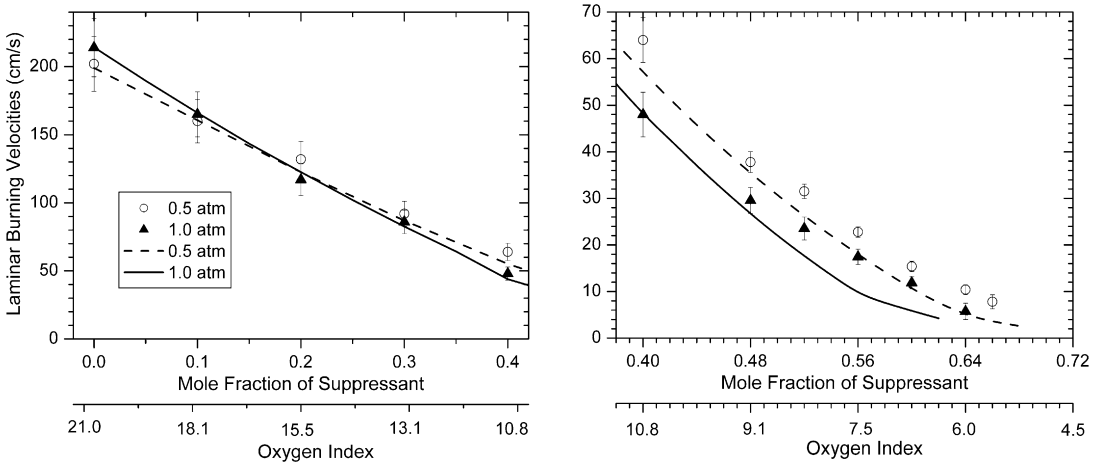

Fig. 5. Measured (symbols) and computed (lines) planar laminar burning velocities as a function of the mole fractions of N_2 suppressants for premixed stoichiometric H_2/air/suppressant flames at pressures of 0.5 and 1.0 atm, obtained from measurements in $1g$ (left) and μg (right).

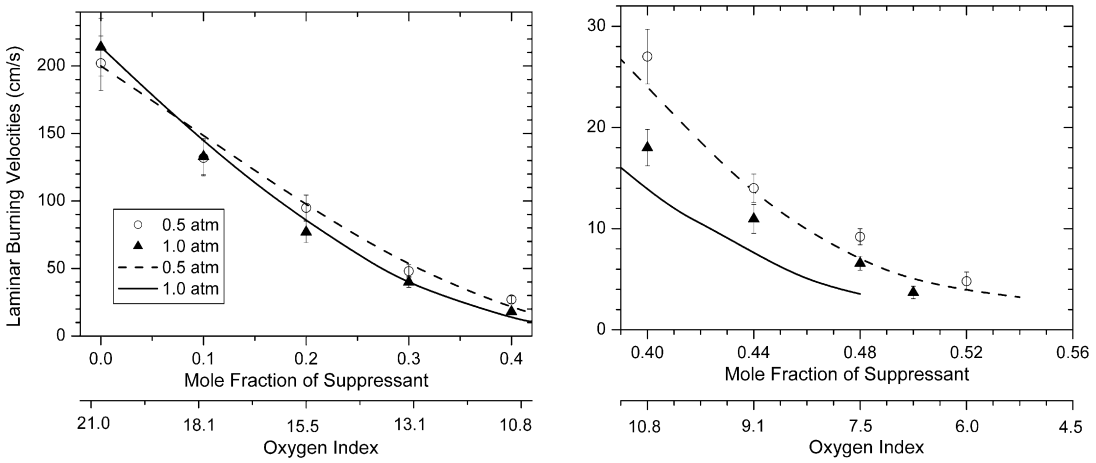

Fig. 6. Measured (symbols) and computed (lines) planar laminar burning velocities as a function of the mole fractions of CO_2 suppressants for premixed stoichiometric H_2/air/suppressant flames at pressures of 0.5 and 1.0 atm, obtained from measurements in $1g$ (left) and μg (right).

note that for a given suppressant concentration, $S_{L\infty}$ at $\phi = 1.8$ (Fig. 4) is generally larger than $S_{L\infty}$ at $\phi = 1.0$ (Fig. 3). This trend is reversed, however, when the suppressant concentration is extremely high and the extinction limit is approached. In the near-limit region, for a given suppressant concentration, $S_{L\infty}$ at $\phi = 1.8$ is lower than that at $\phi = 1.0$. This suggests that factors other than the H radical concentration in the reaction zone become important in determining $S_{L\infty}$. For example, the lower flame temperature could reduce $S_{L\infty}$. This is a topic for further study.

As can be seen in Figs. 3 and 4, the measured and computed values of $S_{L\infty}$ are close when $S_{L\infty}$ is high and diluent concentrations are low. The agreement is less satisfactory for the near-limit mixtures with low $S_{L\infty}$ and high diluent concentrations. For all diluents, the measured near-limit values are higher than computations for $\phi = 1.0$, but lower for $\phi = 1.8$. The discrepancy increases as the diluent concentration is increased. As discussed below, this near-limit discrepancy could arise from uncertainties in chemical reaction rates and transport properties used in the calculations.

Figs. 5 and 6 show the measured and calculated values of $S_{L\infty}$ as a function of the diluent mole fraction for stoichiometric H_2/air flames at pressures of 0.5 and 1.0 atm, respectively. Fig. 5 considers the effect of additional nitrogen added as a suppressant, and Fig. 6 considers carbon dioxide as a suppressant. The results are similar to those in Fig. 3. The comparison

between the measurements and simulations is excellent far away from the flammability limits, but the measured velocities are higher than the computed values in the near-limit region. The suppressants again progressively reduce $S_{L\infty}$ as their concentrations are increased, with CO_2 more effective than N_2.

As shown in both Figs. 5 and 6, for fast (i.e., unsuppressed or slightly suppressed) flames, there is a slight increase in $S_{L\infty}$ as the pressure increases. For relatively slow flames (i.e., diluent concentrations above 20%), however, increasing pressure actually decreases $S_{L\infty}$. This opposite trend is mainly due to the competition between the temperature-sensitive 2-body chain-branching reactions and the pressure-sensitive 3-body chain-termination reactions. Generally, increasing pressure increases flame temperature and increases the global reaction rate, specifically for the termination reactions $H + O_2 + M = HO_2 + M$. These fast flames have high flame temperatures, and thus chain-branching reactions dominate over chain-termination reactions, resulting in an increase of $S_{L\infty}$ as pressure increases. Slow flames (i.e., generally having $S_{L\infty}$ below roughly 150 cm/s), however, have low flame temperatures and are sensitive to the effect of pressure on the rates of 3-body termination reactions. Thus, an increase of pressure decreases the concentration of free radicals in the reaction zone, resulting in a decrease of $S_{L\infty}$.

The next question concerns the effects of pressure on flammability limits. The extinguishing mole fractions of each diluent at 0.5 and 1.0 atm were measured. For example, the mole fractions of N_2 at extinction (in the reactant mixture) are 69% at 0.5 atm and 67% at 1.0 atm for H_2/air flames. This means that the extinguishing mole fraction of a suppressant at 0.5 atm is only slightly higher than that at 1.0 atm. It should be noted that suppressant concentration required for extinguishing a flame is proportional to pressure. Therefore, much less suppressant is actually needed at 0.5 atm than that at 1.0 atm. This indicates that it is easier to extinguish a fire at reduced pressure.

5. Flame instabilities

Preferential-diffusion and hydrodynamic instabilities were observed in the present experiments. The preferential-diffusion instability is more important because it involves interactions between effects of preferential-diffusion and flame stretch. Its presence is identified relatively early in the flame-propagation process by irregular distortions of the flame surface. It was only observed for flames with negative Markstein numbers, where it eventually causes flame wrinkling. Flame surfaces, however, remained smooth at small radii so that laminar burning velocities could still be measured at early times, even at these conditions. The hydrodynamic instability resulted in cellular patterns on the flame surface, and these occurred later in the flame-propagation process. What we observed is very similar to what is reported by Groff [20]. Because the hydrodynamic instability only occurred at relatively large flame radii, they did not affect the present measurements of flame radius $r_f(t)$, which were restricted to earlier times. In previous normal-gravity experiments, the buoyancy-induced instability, characterized by nonspherical flame surfaces and upward motions of the centroids of flames, was observed for slow near-limit flames.

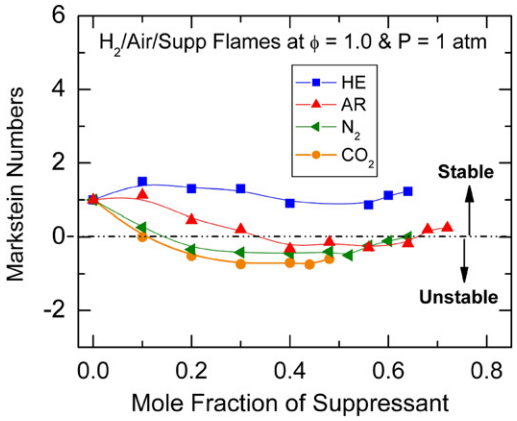

Fig. 7. Measured Markstein numbers as a function of the mole fraction of He, Ar, N_2, and CO_2 suppressants for premixed stoichiometric H_2/air/suppressant flames at 1.0 atm pressure.

It is well known that lean H_2/air flames are intrinsically unstable, and rich H_2/air flames are stable, as a result of preferential diffusion [5,21]. Generally, laminar premixed flames are unstable because of preferential diffusion when the fast-diffusing component, H_2 in the current experiments, is deficient. For stoichiometric H_2/air mixtures, however, we found that the addition of suppressants can change the preferential-diffusion instability. Fig. 7 shows measured Markstein numbers as a function of the mole fraction of suppressant for stoichiometric H_2/air flames at NTP. Away from the limits, and with the exception of helium, Ma decreases as the concentration of suppressant increases. This trend is consistent with the conclusion that addition of chemically active suppressants (halons) also tend to decrease the Markstein numbers [22]. In these cases, the preferential-diffusion instability is promoted as the flame becomes more suppressed. N_2 and Ar dilution have similar effects on the variation of Ma. This is mainly due to their similar transport properties ($D_u = 72.9$ mm^2/s for N_2-diluted flames and $D_u = 76.9$ mm^2/s for Ar-diluted flames, based on the binary diffusivity of H_2–

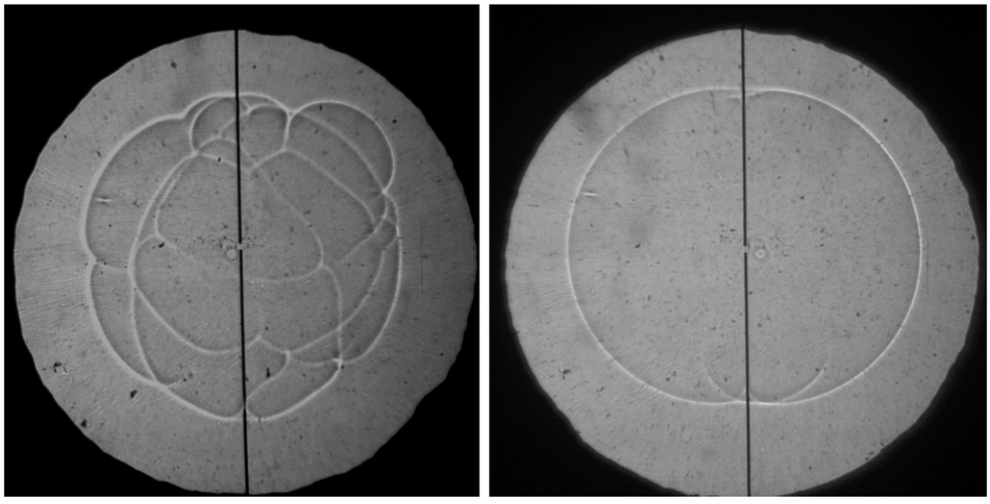

Fig. 8. Shadowgraph images of two near-limit flames: (a) stoichiometric H_2/air/50% CO_2 flame at NTP (unstable); (b) stoichiometric H_2/air/72% Ar flame at NTP (stable).

N_2 or H_2–Ar at NTP). At the near-limit suppressant concentrations, the Ar mixture has a slightly positive Markstein number, which represents stable preferential-diffusion condition. The N_2 mixture is almost neutrally stable. The CO_2 mixture has a negative Markstein number, which represents an unstable condition.

Results for He as a suppressant differ from this general behavior, however, because the transport properties of He-diluted flames are significantly different from those of N_2-, Ar-, or CO_2-diluted flames. For example, the mass diffusivity increases with helium addition ($D_u = 158.7$ mm^2/s for He-diluted flames at NTP). A more significant effect is the increase of thermal diffusivity of the mixture in the helium-diluted case as a result of the enhanced thermal conductivity of helium (roughly five times higher than that of N_2 in the temperature range 300–3000 K). The high thermal conductivity of the fast-diffusing He molecules tends to promote preferential diffusion of the reaction zone and thus stability of the flames to preferential-diffusion/stretch interactions.

Fig. 8 shows shadowgraph images of two near-limit flames that both correspond to $\phi = 1.0$ and $p = 1$ atm, namely H_2/air/50% CO_2 and H_2/air/72% Ar. These flames have approximately equal laminar burning velocities ($S_{L\infty}$ is about 6 cm/s), although the wrinkled flame is unstable and the smooth flame is stable. For stoichiometric combustion of H_2 and air at NTP, the flame is stable. Addition of CO_2 or Ar both decreases Ma and promotes preferential-diffusion instability. This effect is more significant for CO_2 than for Ar or N_2. The high concentration of CO_2 causes both the thermal and mass diffusivity of the reactant mixture to decrease. The decrease in thermal diffusivity, however, is more significant than the decrease in mass diffusivity. Thus the Lewis number of the mixture decreases as the CO_2 concentration increases, and the flame tends to become more unstable.

Overall, the effect of chemically inert diluents, especially CO_2, on premixed flames involves two counteracting effects. Diluents have the ability to reduce H and OH radical concentrations in the reaction zone, which tends to reduce the laminar burning velocities and suppress the flame [1]. The same ability of diluents to reduce H and OH radical concentrations in the reaction zone, however, also enhances the potential for the development of preferential-diffusion-induced flame surface instabilities. The resulting flame surface wrinkling for unstable flames leads to increased flame surface area, and thus an increase in the burning rate. The latter effect can offset the intended effect of the suppressant in reducing the overall burning rate.

6. Sensitivity analysis

As shown in Figs. 3–6, the present measurements and calculations for unstretched laminar burning velocity agree well at low diluent concentrations, but they diverge at higher concentrations as the observed extinction limits are approached. For stoichiometric flames, the calculations predict lower burning velocities, whereas for fuel-rich ($\phi = 1.8$) flames, they predict higher velocities. These results are consistent with the work of Egolfopoulos and Law [23] and Wu et al. [24]. In fact, Wu et al. [24] tested a number of different chemical kinetic models which all gave

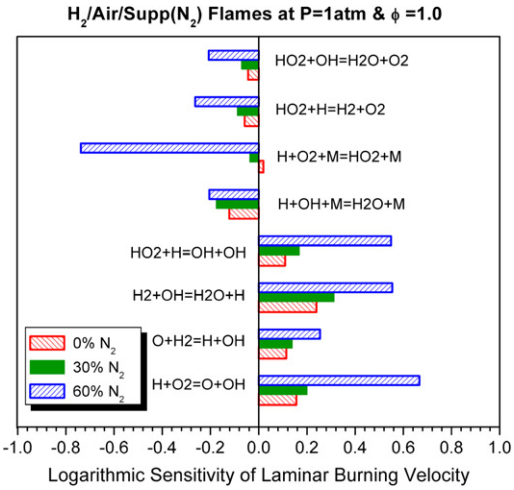

Fig. 9. Logarithmic sensitivity coefficients of laminar burning velocity with respect to reaction rate coefficients, computed for stoichiometric H_2/air flames having 0% N_2, 30% N_2, and 60% N_2 as suppressants at 1.0 atm, respectively, using the kinetics of Li et al. [8].

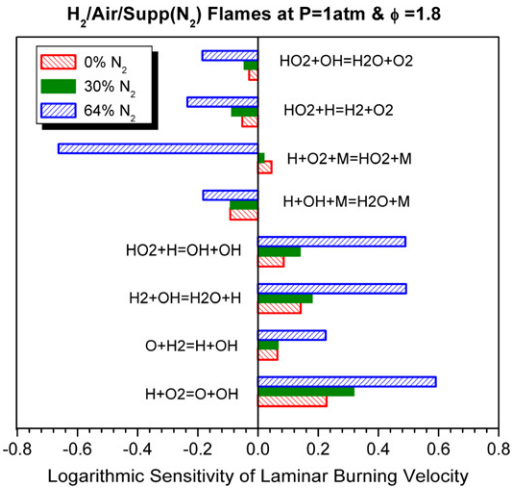

Fig. 10. Logarithmic sensitivity coefficients of laminar burning velocity with respect to reaction rate coefficients, computed for H_2/air flames having 0% N_2, 30% N_2, and 64% N_2 as suppressants at a fuel equivalence ratio of 1.8 and a pressure of 1.0 atm, respectively, using the kinetics of Li et al. [8].

the same results for stoichiometric flames and different results near the lean or rich limits. There is also evidence that the effects of uncertainties on molecular diffusion coefficients are significant in computing hydrogen flame-extinction process [25]. Sensitivity analyses can be useful in sorting out these dependencies.

6.1. Chemical kinetics

A sensitivity analysis of laminar burning velocities with respect to reaction rate coefficients was performed for stoichiometric H_2/air flames at three different levels of nitrogen dilution (0%, 30%, and 60% N_2 by volume in the reactant mixture). The results are summarized in Fig. 9. A positive sensitivity coefficient indicates that increasing the reaction rate increases $S_{L\infty}$. Conversely, a negative coefficient means that increasing the reaction rate decreases $S_{L\infty}$.

The results show that the laminar burning velocity is positively sensitive to the reactions $HO_2 + H = OH + OH$, $H_2 + OH = H_2O + H$, $O + H_2 = H + OH$ and the chain-branching reaction $H + O_2 = O + OH$. On the other hand, the chain-termination reactions $H + OH + M = H_2O + M$, $H + O_2 + M = HO_2 + M$, $HO_2 + H = H_2 + O_2$, and $HO_2 + OH = H_2O + O_2$ have negative sensitivity. Increasing the dilution (N_2) mole fraction increases the corresponding sensitivities, yielding the highest sensitivities at the largest N_2 mole fraction.

For the undiluted (0% N_2) or moderately diluted (30% N_2) flames, the 2-body chain-branching reactions are dominant, while the 3-body chain-termination reactions $H + O_2 + M = HO_2 + M$ are much less important. The 3-body chain-termination reactions, however, become significantly important for the near-limit flame (60% N_2 dilution). The magnitude of the sensitivity to $H + O_2 + M = HO_2 + M$ is on the same order as, but larger than, the sensitivity to chain-branching reactions. This indicates that, as the extinction limit is approached, the $H + O_2 + M = HO_2 + M$ increasingly controls the flame. A similar conclusion was found for H_2/air/diluent flames at $\phi = 1.8$, as shown in Fig. 10. Egolfopoulos and Law [23] show that the 2-body chain-branching reactions shift to 3-body chain-termination reactions as pressure increases, because the 3-body reactions are pressure-sensitive while the 2-body reactions are temperature-sensitive. Here, we find the $H + O_2 + M = HO_2 + M$ reaction also becomes relatively more important as dilution increases. This is mainly because a high concentration of M lowers the flame temperature, which, in turn, significantly reduces the rate of chain branching reactions.

Figs. 9 and 10 suggest the possibility that a substantial part of the discrepancy between the measured and computed laminar burning velocities in Figs. 3–6 may be due to the three-body recombination rates for $H + O_2 + M = HO_2 + M$ reactions, and in particular to the third-body collision efficiency of various species M. To further identify the effects of various third-bodies, we performed a sensitivity analysis of $S_{L\infty}$ with respect to the third-body collision efficiency of various species M for the near-

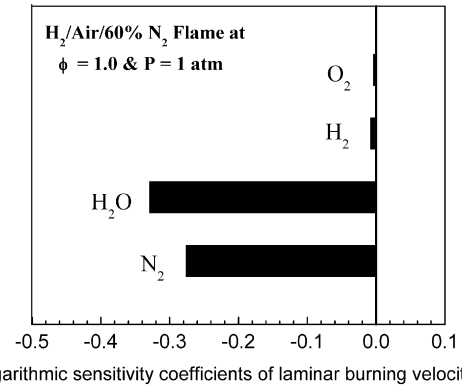

Fig. 11. Logarithmic sensitivity coefficients of laminar burning velocity with respect to the third-body collision efficiency of various species M in the H + O_2 + M = HO_2 + M reactions, computed for stoichiometric H_2/air/60% N_2 flame at 1.0 atm, using the kinetics of Li et al. [8].

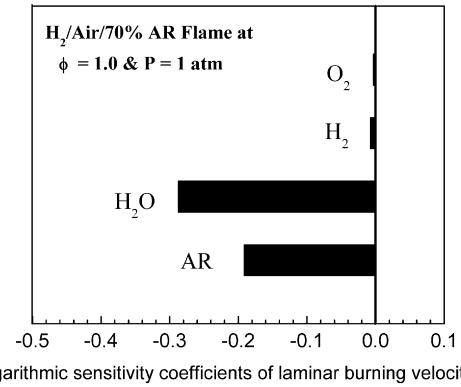

Fig. 12. Logarithmic sensitivity coefficients of laminar burning velocity with respect to the third-body collision efficiency of various species M in the H + O_2 + M = HO_2 + M reactions, computed for stoichiometric H_2/air/70% Ar flame at 1.0 atm, using the kinetics of Li et al. [8].

limit stoichiometric H_2/air/60% N_2 flame, as shown in Fig. 11. This was done by performing a series of calculations that perturb the third-body collision efficiency C_{Ti} of species i, which were then used to compute logarithmic sensitivities by computing derivatives $\partial(\ln S_{L\infty})/\partial(\ln C_{Ti})$. Fig. 11 shows that $S_{L\infty}$ is most sensitive to the third-body efficiency of H_2O, and is second most sensitive to the efficiency of N_2. Effects of other third bodies are very small. Another near-limit flame containing argon (stoichiometric H_2/air/70% Ar at 1 atm) was also used to identify the effects of various third bodies, as shown in Fig. 12. For this flame, $S_{L\infty}$ is most sensitive to the third-body efficiencies of H_2O and Ar. These suggest potential value in measurements and simulations to better define the third-body efficiencies of H_2O, N_2, and Ar (or He) in this key reaction.

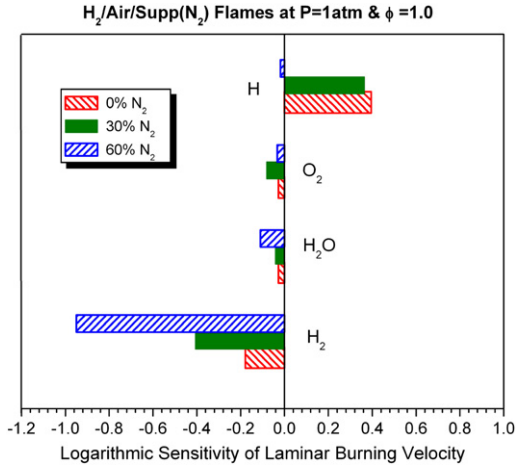

Fig. 13. Logarithmic sensitivity coefficients of laminar burning velocity with respect to mass diffusion coefficients, computed for stoichiometric H_2/air flames having 0% N_2, 30% N_2, and 60% N_2 as suppressants at 1.0 atm, respectively, using the kinetics of Li et al. [8].

6.2. Molecular diffusion

The standard PREMIX code automatically outputs the logarithmic sensitivity coefficients $\partial(\ln S_{L\infty})/\partial(\ln A)$ of $S_{L\infty}$ with respect to all reaction rate coefficients A. PREMIX cannot directly compute the sensitivity of species diffusivities. The effect of the mass diffusion coefficient of each species i to the mixture, $D_{i,m}$, on $S_{L\infty}$ was evaluated from a series of calculations that perturbed the mass diffusion coefficients in question. These results then were used to compute logarithmic sensitivities by determining the derivatives $\partial(\ln S_{L\infty})/\partial(\ln D_{i,m})$.

For a direct comparison of the sensitivities to mass diffusion coefficients and those to chemical kinetics, we chose the same flame conditions as above. The results are shown in Fig. 13. The mass diffusivities of four species, H_2, H_2O, O_2, and H, especially H_2 and H radical, have a notable effect on $S_{L\infty}$. The sensitivities of the mass diffusion of H_2, H_2O, and O_2 are negative for all three flames, whereas the sensitivity of the mass diffusion of the H radical is negative for the flame without suppressant but positive for the flames with suppressant.

The negative sensitivity of the H_2 diffusion coefficient can be explained as follows. For one-dimensional, freely propagating flames, the thickness of the diffusive layer of any reactant i, δ_i, scales with $D_{i,m}$ according to the relation $\delta_i \sim D_{i,m}^{3/2}$ [25]. An increase in the diffusivity of H_2 leads to a greater increase in the thickness of the H_2 diffusive layer, which in turn results in weaker H_2 concentration gradients. The flux of H_2 into the flame zone is proportional to the product of the diffusion coefficient and the concentration

gradient. The decrease in the concentration gradient overwhelms the increase in diffusivity. This results in an overall decrease in the flux of H_2 to the flame. Thus, the sensitivities of the diffusivity of H_2 and laminar burning velocity are inversely related.

The sensitivity of $S_{L\infty}$ to mass diffusion of H_2 significantly increases as dilution increases and the extinction limit is approached, as shown in Fig. 13. This is because for more diluted flames, the H_2 concentration is low and the overall reactivity is controlled more by diffusion. At the limit (H_2/air/60% N_2 flame), $S_{L\infty}$ has a high sensitivity to the mass diffusion of H_2, which is even higher than those to the chain-branching reactions and the 3-body chain-termination reactions shown in Fig. 9. Thus it is possible that uncertainties related to mass diffusion (in particular to the mass diffusion of H_2) and chemical kinetics (in particular the 3-body chain-termination $H + O_2 + M = HO_2 + M$ reactions) could both contribute to the discrepancies in the near-limit laminar burning velocities between the experiments and simulations.

7. Radiation heat loss

Numerous studies have considered how dilution may lead to extinction via heat losses by radiation or thermal conduction. Increasing dilution decreases the flame temperature and thus increases the impact of heat loss, which eventually leads to a flammability limit. In the microgravity experiments described here, the 180 mm radius of the spherical chamber was sufficiently large in comparison with the $r_f < 30$ mm flames for heat losses by conduction to the walls or to the 250-μm tungsten electrodes to be negligible. Therefore, heat loss by radiation is probably the dominant extinction loss mechanism. Fig. 14 shows burning velocities as a function of suppressant (N_2 or CO_2) mole concentration, computed both without accounting for radiation loss and with an optically thin radiation model. The results indicate that radiative heat loss can be neglected for fast-propagating CO_2 flames. It can, however, reduce the laminar burning velocity significantly as the flame slows and the flammability limit is approached, because CO_2 is a strong radiating species. For N_2-diluted flames, however, the difference for results with and without radiation loss is very small, even in the near-limit region.

The optically thin assumption is appropriate for H_2/air flames with N_2, Ar, and He suppressants for which the main radiating species is H_2O. The effects of radiation absorption might need to be taken into account for CO_2-diluted flames because CO_2 is a strong absorber. Ju et al. [26] and Guo et al. [27] found that radiation absorption leads to a higher flame

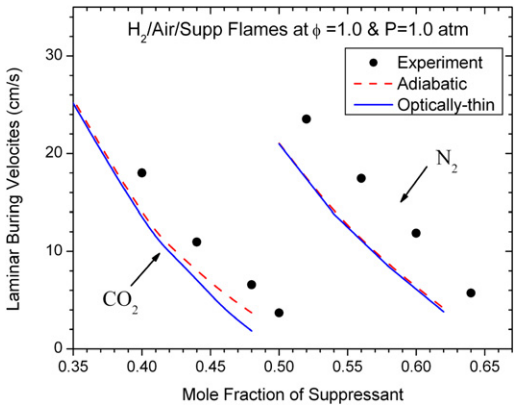

Fig. 14. Measured (symbols) and computed (lines) laminar burning velocities as a function of the mole fraction of N_2 or CO_2 suppressant for stoichiometric H_2/air/N_2 or CO_2 flames with (solid) and without (dashed) radiation heat loss.

temperature and burning velocity than the adiabatic flame. A fundamental flammability limit can exist due to radiative heat losses, but such a limit is strongly dependent on the emission–absorption spectra of the reactant and product gases and their temperature dependence. It could not be predicted using gray-gas or optically thin models. In the results presented here, we used an optically thin assumption that does not include reabsorption effects of CO_2. Nevertheless, our microgravity experiments provide low near-limit burning velocities of CO_2 mixtures, and in the future these can be compared to radiation models with absorption.

8. Conclusions

The effects of diluents on the near-limit properties of microgravity hydrogen flames were investigated using a short-drop free-fall laboratory facility. The experiments involved unsteady outwardly propagating spherical laminar premixed hydrogen/air flames at various fuel equivalence ratios and pressures with He, Ar, N_2, and CO_2 as chemically passive gaseous suppressants at varying concentrations. Corresponding calculations of laminar burning velocities considered variable transport and thermodynamic properties, a radiation model, and the detailed H_2/O_2 chemical kinetic mechanism of Li et al. [8]. The major conclusions from this investigation are as follows:

(1) Consistent with our earlier work [2], the suppressants increase in effectiveness based on the reduction of $S_{L\infty}$ for a given molar concentration of suppressant in the order He, Ar, N_2, and CO_2. This reflects both their progressively increasing specific heats and progressively decreasing mass and thermal transport properties.

(2) Consistent with the earlier studies in this group [1,22], there is a tendency for the addition of suppressants, either chemically active (halons) or chemically passive (except helium), to reduce the Markstein number for a given reactant mixture. This indicates that suppressed flames are more susceptible to preferential-diffusion instabilities. Wrinkled unstable flames have increased burning rates due to the increased surface area for reaction. Thus the tendency of fire suppressants to reduce laminar burning velocities, and thus act to reduce the severity of unwanted fires, is counteracted to some extent by their tendency to reduce Markstein numbers and thereby promote flame instabilities that can increase the severity of unwanted fires. This is an undesirable effect of flame suppressants with respect to fire safety.

(3) Reducing pressure decreases $S_{L\infty}$ for fast flames, but increases $S_{L\infty}$ for slow flames. These opposing trends are mainly due to the competition between the temperature-sensitive 2-body chain-branching reactions and the pressure-sensitive 3-body chain-termination reactions. Although the flammability limit is extended at reduced pressure, less suppressant is actually needed to suppress a fire. In this sense it is easier to extinguish a fire at reduced pressures.

(4) Measured and computed values for $S_{L\infty}$ agree well at low suppressant concentrations, but diverge at higher concentration as the observed extinction limits are approached. Specifically, for stoichiometric flames, the simulations predict lower burning velocity, whereas for fuel-rich ($\phi = 1.8$) flames, the simulations predict higher velocity. Sensitivity analyses suggest that the uncertainties related to mass diffusion coefficients, particularly the mass diffusion of H_2, and the uncertainties in the 3-body chain-termination $H + O_2 + M = HO_2 + M$ reaction rates, could both contribute to the near-limit discrepancies.

Acknowledgments

This research was supported by NASA Grant NNC04GA08G, with Dr. F. Takahashi of NASA Glenn Research Center serving as program manager. Support from the Rackham Predoctoral Fellowship at the University of Michigan is also acknowledged. The authors would like to thank Dr. K. Kailasanath at NRL and Professor Y. Ju at Princeton University for inspiring discussions.

References

[1] L. Qiao, C.H. Kim, G.M. Faeth, Combust. Flame 143 (2005) 79–96.

[2] L. Qiao, Y. Gu, W.J.A. Dahm, E.S. Oran, G.M. Faeth, Proc. Combust. Inst. 31 (2007) 2701–2709.

[3] R.A. Strehlow, L.D. Savage, Combust. Flame 31 (1978) 209–211.

[4] B.J. McBride, M.A. Reno, S. Gordon, CET93 and CETPC: An Interim Updated Version of the NASA Lewis Computer Program for Calculating Complex Chemical Equilibrium with Applications, NASA TM 4557, 1994.

[5] G.H. Markstein, Non-Steady Flame Propagation, Pergamon, New York, 1964, p. 22.

[6] P. Clavin, Prog. Energy Combust. Sci. 11 (1985) 1–59.

[7] R.J. Kee, F.M. Rupley, J.A. Miller, The CHEMKIN Thermodynamic Data Base, Report SAND87-8215B, Sandia National Laboratories, 1992.

[8] J. Li, Z. Zhao, A. Kazakov, F.L. Dryer, Int. J. Chem. Kinet. 36 (2004) 1–10.

[9] R.J. Kee, J.F. Grcar, M.D. Smooke, J.A. Miller, A FORTRAN Program for Modeling Steady Laminar One-Dimensional Premixed Flames, Report SAND85-8240, Sandia National Laboratories, Albuquerque, NM, 1993.

[10] T.J. Kim, R.A. Yetter, F.L. Dryer, Proc. Combust. Inst. 25 (1994) 759–766.

[11] K.T. Aung, M.I. Hassan, G.M. Faeth, Combust. Flame 109 (1997) 1–24.

[12] K.T. Aung, M.I. Hassan, G.M. Faeth, Combust. Flame 112 (1998) 1–15.

[13] Y. Ju, H. Guo, F. Liu, K. Maruta, J. Fluid Mech. 379 (1999) 165–190.

[14] W.S. Cleveland, The Elements of Graphing Data, Wadsworth, Monterey, CA, 1985, pp. 167–178.

[15] C.K. Law, G.M. Faeth, Prog. Energy Combust. Sci. 20 (1994) 65–113.

[16] N. Saito, Y. Ogawa, Y. Saso, C. Liao, R. Sakei, Fire Safe. J. 27 (1996) 185–200.

[17] Y. Saso, N. Saito, C. Liao, Y. Ogawa, Fire Safe. J. 26 (1996) 303–326.

[18] F. Takahashi, G.T. Linteris, V.R. Katta, Proc. Combust. Inst. 31 (2007) 2721–2729.

[19] O.C. Kwon, G.M. Faeth, Combust. Flame 124 (2001) 590–610.

[20] E.G. Groff, Combust. Flame 48 (1982) 51–52.

[21] J. Manton, G. von Elbe, B. Lewis, J. Chem. Phys. 20 (1952) 153–157.

[22] G.M. Faeth, C.H. Kim, O.C. Kwon, Clean Air 4 (2003) 115–187.

[23] F.N. Egolfopoulos, C.K. Law, Proc. Combust. Inst. 23 (1990) 333–340.

[24] M.S. Wu, J.B. Liu, P.D. Ronney, Proc. Combust. Inst. 27 (1998) 2543–2550.

[25] Y. Dong, A.T. Holley, M.G. Andac, F.N. Egolfopoulos, S.G. Davis, P. Middha, H. Wang, Combust. Flame 142 (2005) 374–387.

[26] Y. Ju, G. Masuya, P.D. Ronney, Proc. Combust. Inst. 27 (1998) 2619–2626.

[27] H. Guo, Y. Ju, K. Maruta, T. Niioka, F. Liu, Combust. Sci. Technol. 135 (1998) 49–64.